June 4, 2009
LA-UR-09-02131
arXiv:yymm.nnnn

Some Radiative Corrections to Neutrino Scattering: I Neutral Currents

James P. Jenkins* and T. Goldman†

Theoretical Division, Los Alamos National Laboratory, Los Alamos, NM 87545

Abstract

With the advent of high precision neutrino scattering experiments comes the need for improved radiative corrections. We present a phenomenological analysis of some contributions to the production of photons in neutrino neutral current scattering that are relevant to experiments subsuming the 1% level.

*Electronic address: jjenkins6@lanl.gov
†Electronic address: tgoldman@lanl.gov

I. INTRODUCTION

Recent neutrino scattering experiments, particularly those searching for electron neutrino appearance [1, 2, 3] by oscillation from muon neutrino beams, report signals below the 1% level. Such unprecedented levels of sensitivity demand corresponding efforts to determine backgrounds. Radiative corrections are clearly expected at this level.

Many years ago, phenomenological analyses of radiative corrections were applied to studies of pion decay [4, 5], to constrain corrections to the weak interaction from non-V-A currents. Their accuracy was confirmed by precise calculations when the Standard Model became established.

Although many contributions are possible, obviating unambiguous predictions, similar phenomenological analyses can provide overall scale, energy and angular distributions for photon production in neutrino scattering. Such methods were used in [6, 7] to help explain the Gargamelle single photon signal [8]. Armed with these predictions, experimental results can then be used to determine whether the total of such contributions are significant within each experiment.

Of course, Monte Carlo calculations by experimental groups include bremsstrahlung from charged particles in the final state and radiative decays of N^* and Δ resonances. However, these are s-channel effects. We consider here photons produced from the particles being exchanged in the t-channel, and so less obviously connected to the external line quanta. In general, such contributions are necessary simply to maintain gauge invariance.

We provide here two examples of amplitudes relevant to neutral current neutrino scattering, which are especially important when distinguishing final state electrons and photons is difficult. We eschew details such as interferences between different contributions, as the final state distributions in our examples differ significantly, minimizing the overlap. (In addition, it is usually the case that possible interfering contributions involve the exchange of much higher mass particles with much smaller phenomenological couplings [9]; hence, interference effects are expected to be minimal.) Our goal is simply to provide experimental groups with distribution formulas that they can use to extract these contributions or determine limits on them.

We provide results for both neutrino and antineutrino scattering. Our results may be easily extended to other similar contributions both in neutral and charged current scattering. Although we focus on modest energy studies, our results are fully relativistically covariant and thus may be applied to any energy. Additional contributions or Regge trajectory generalizations of the meson exchanges are likely necessary for application to very high energies. Our results are also straightforwardly generalizable to other related processes such as charged current interactions, which we will present elsewhere.

II. LAGRANGIAN

Photon production in neutral current neutrino scattering produces a background to the identification of electron neutrino events in (generally non-magnetic) detectors which distinguish poorly between electrons and photons. Standard radiative corrections, such as those due to bremsstrahlung of a photon from charged particles in the target or final state, have been closely examined previously [10]. See also [11, 12] and references therein. Additional processes, such as production of a Δ baryon or N^* followed by its decay back to a nucleon and a photon [13], are also already included in many experimental Monte Carlo assessments of backgrounds [9].

Recently, however, a "new" triangle anomaly has been identified in reference [14], hereinafter referred to as H3, which can contribute a previously unconsidered source of such background. However, the structure of that contribution is very similar to a phenomenological contribution which we display in Fig.(1). Here the Z-boson carrying the neutral current interaction from the neutrino line mixes into a vector boson, in the familiar fashion of Vector Meson Dominance (VMD). [15] In this case, the hadronic vector meson is an ω (or a ρ^0) which undergoes a virtual decay to the photon of interest and a pion in the t-channel. This last couples strongly to the hadron target (nucleon or nucleus) completing the interaction.

The advantage over the H3 approach is that the vertex strength is known phenomenologically from the rate of the decay

$$\omega \to \pi^0 + \gamma$$

and similarly for the ρ^0 case. The pion coupling to the nucleon is also well-known [16]. The strength of the $Z-\omega$ mixing is determined by VMD and the off-shell variation of this mixing

is easily determined by a well-known extension [17, 18], originally worked out for the case of isospin violating contributions to the nuclear force. We explicitly calculate the appropriate analog in Appendix (A 2) for completeness.

No other parameters are required, so the prediction of the contribution to the total cross section for producing a final state photon is absolute for this graph. We emphasize that the structure of the central vertex has the same vector-vector-axial-vector coupling structure as in H3, due to the axial vector nature of the pion current. However, in our approach, all of the strong interaction corrections (higher order in QCD and quark-antiquark "resonance" effects) relevant to the triangle graph of H3 are fully taken into account phenomenologically. Of course, other similar contributions occur with vector-meson recurrences, etc., but these predominantly affect only the overall strength, and furthermore, experience has shown that at the modest energies of the experiments of interest (LSND [1] and MiniBooNE [2, 3]), the sum over all such contributions is likely to be dominated by these leading ones.

The interaction Lagrangian terms needed in our approach are:

$$\mathcal{L}_I = e g_{\omega\gamma\pi} \epsilon_{\mu\nu\xi\sigma} \omega^\mu \partial^\nu \pi^0 F^{\xi\sigma} + g_{\pi NN} \bar{\Psi} \gamma^\mu \partial_\mu \vec{\pi} \cdot \vec{\tau} \Psi \tag{1}$$

where Ψ is the nucleon field and $\vec{\tau}$ is the vector of usual isospin generators.

We also make use of the usual Standard Model weak interaction couplings of the Z-boson to neutrinos and to quarks. The last are needed to compute the off-shell variation of the VMD mixing between the Z and the ω. The $\omega - \pi - \gamma$ coupling constant, $g_{\omega\pi\gamma} = e g_\omega$ (with the explicit factor of the electromagnetic coupling, e, stripped out for clarity) is determined from the experimental value of the (on-shell) radiative $\omega \to \pi + \gamma$ decay rate, shown in Appendix (A 1). We will discuss possible off-shell effects on this compared with the corresponding effects for the H3 approach in our discussion section (IV).

III. CROSS SECTION

We consider the process shown in Fig.1. In terms of the labeled momentum 4-vectors, the squared amplitude is

$$\mathcal{A}^2 = \frac{128 M_n^2 g_{\nu Z}^2 g_{\omega\gamma\pi}^2 g_{\pi NN}^2 g_{\omega Z}^2(q^2)}{(q^2 - M_Z^2)^2 (q^2 - M_\omega^2)^2 (Q^2 - M_\pi^2)^2} \ell_i \cdot \ell_f (p_i \cdot p_f - M_N^2) \left((k \cdot \ell_i)^2 + (k \cdot \ell_f)^2 \right), \tag{2}$$

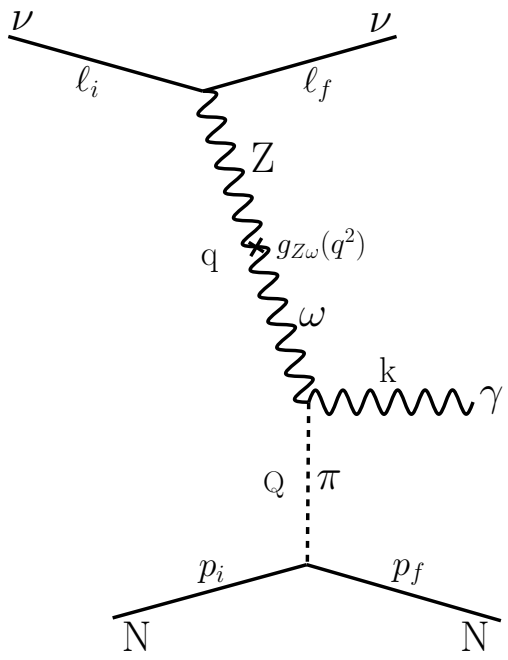

FIG. 1: Specific diagram considered in this analysis. Variants are discussed in the text.

where the neutrino-Z coupling is given by $g_{\nu Z} = (g/2)\cos\theta_W$ in terms of the $SU(2)$ gauge coupling g. The remaining coupling constants will be discussed in what follows. In the center of mass (CM) frame, the momenta can be written explicitly as

$$\ell_i = (E_{\ell_i}, \vec{E}_{\ell_i}) \tag{3}$$

$$p_i = (E_{p_i}, -\vec{E}_{\ell_i}) \tag{4}$$

$$\ell_f = (E_{\ell_f}, \vec{E}_{\ell_f}) \tag{5}$$

$$p_f = (E_{p_f}, \vec{p}_{p_f}) \tag{6}$$

$$k = (E_k, \vec{E}_k), \tag{7}$$

where we employ the shorthand $\vec{E}_i = \vec{p}_i$ to indicate a massless particle's 3-momentum. To obtain the desired cross-section, we first partially evaluate the phase space integrals by making use of momentum conserving delta functions. We find the differential cross-section for the photon in the final state is

$$\frac{d\sigma}{dE_k d\mu} = \frac{M_N^2 g_{\nu Z}^2 g_{\omega\gamma\pi}^2 g_{\pi NN}^2}{(2\pi)^4 E_{\ell_i}(E_{\ell_i} + E_{p_i})} \int dE_{\ell_f} d\phi \frac{g_{\omega Z}^2(q^2) q^2 Q^2 \left((k\cdot\ell_i)^2 + (k\cdot\ell_f)^2\right)}{(q^2 - M_Z^2)^2 (q^2 - M_\omega^2)^2 (Q^2 - M_\pi)^2}, \tag{8}$$

in terms of its energy (E_k) and opening angle from the beam direction ($\mu = \cos\theta$). Here the t-channel momentum transfers are: $q^2 = -2E_{\ell_i}E_{\ell_f}(1 - \mu_{\ell_f})$ and $Q^2 = q^2 - 2k\cdot\ell_i + 2k\cdot\ell_f$,

where μ_{ℓ_f} is the cosine of the opening angle between the neutrino in the final and initial state. It is related to μ and the cosine $\mu_{\ell_f k}$ of the opening angle between the photon and the final state neutrino by

$$\mu_{\ell_f} = \mu\mu_{\ell_f k} + \sqrt{1-\mu^2}\sqrt{1-\mu_{\ell_f k}^2}\cos\phi. \tag{9}$$

This is the only source of ϕ dependence in the system. Momentum conservation fixes

$$\mu_{\ell_f k} = \frac{1}{2E_{\ell_f}E_k}\left(\sqrt{s}^2 - 2\sqrt{s}(E_{\ell_f}+E_k) + 2E_kE_{\ell_f} - M_N^2\right) \tag{10}$$

as a function of the invariant $\sqrt{s} = E_{\ell_i} + E_{p_i}$. Requiring that $\mu_{\ell_f k} \in \{-1, 1\}$ yields the E_{ℓ_f} integration limits

$$E_{\ell_f}^{\min} = \frac{\sqrt{s}^2 - M_N^2 - 2\sqrt{s}E_K}{2\sqrt{s}} \tag{11}$$

$$E_{\ell_f}^{\max} = \frac{\sqrt{s}^2 - M_N^2 - 2\sqrt{s}E_K}{2\sqrt{s} - 4E_k}. \tag{12}$$

Additionally, we require $E_k \leq \frac{1}{2\sqrt{s}}(\sqrt{s}^2 - M_N^2)$ to maintain positive values for these energies. The $\omega - Z$ mixing coupling function, $g_{\omega Z}^2(q^2)$, is found from the self energy diagram in Fig.7 of Appendix (A 2). It is almost constant in the space-like regime where it is needed here.

Taking the limit $|q^2| \ll M_Z^2$ and $|Q^2| \gg M_\pi^2$, the cross section simplifies to

$$\frac{d\sigma}{dE_k d\mu} = \frac{M_N^2 g_{\nu Z}^2 \bar{g}_{\omega Z}^2 g_{\omega\gamma\pi}^2 g_{\pi NN}^2}{(2\pi)^4 E_{\ell_i}(E_{\ell_i}+E_{p_i})M_Z^4}\int dE_{\ell_f}\left((k\cdot\ell_i)^2 + (k\cdot\ell_f)^2\right)\int d\phi \frac{q^2}{Q^2(q^2-M_\omega^2)^2}, \tag{13}$$

where we have neglected the q^2 dependence of $g_{\omega Z}$ and assume an average value. Integrating over ϕ, we obtain

$$\begin{aligned}\frac{d\sigma}{dE_k d\mu} &= \frac{M_N^2 E_k^2 g_{\nu Z}^2 \bar{g}_{\omega Z}^2 g_{\omega\gamma\pi}^2 g_{\pi NN}^2}{(2\pi)^3 E_{\ell_i}(E_{\ell_i}+E_{p_i})M_Z^4}\int dE_{\ell_f}\left(E_{\ell_i}^2(1-\mu)^2 + E_{\ell_f}^2(1-\mu_{\ell_f k})^2\right) \\ &\times \frac{1}{f^2(b-c)^2}\left\{\frac{a-b}{(b^2-1)^{\frac{1}{2}}} + \frac{c^3-2ac^2+abc-b+a}{(c^2-1)^{\frac{3}{2}}}\right\},\end{aligned} \tag{14}$$

where we have introduced

$$f = 2E_{\ell_i}E_{\ell_f}\sqrt{1-\mu^2}\sqrt{1-\mu_{\ell_f k}^2} \tag{15}$$

$$a = \frac{2E_{\ell_i}E_{\ell_f}(1-\mu\mu_{\ell_f k})}{f} \tag{16}$$

$$b = \frac{2E_{\ell_i}E_{\ell_f}(1-\mu\mu_{\ell_f k}) + 2E_kE_{\ell_i}(1-\mu) - 2E_kE_{\ell_f}(1-\mu_{\ell_f k})}{f} \tag{17}$$

$$c = \frac{2E_{\ell_i}E_{\ell_f}(1-\mu\mu_{\ell_f k}) + M_\omega^2}{f} \tag{18}$$

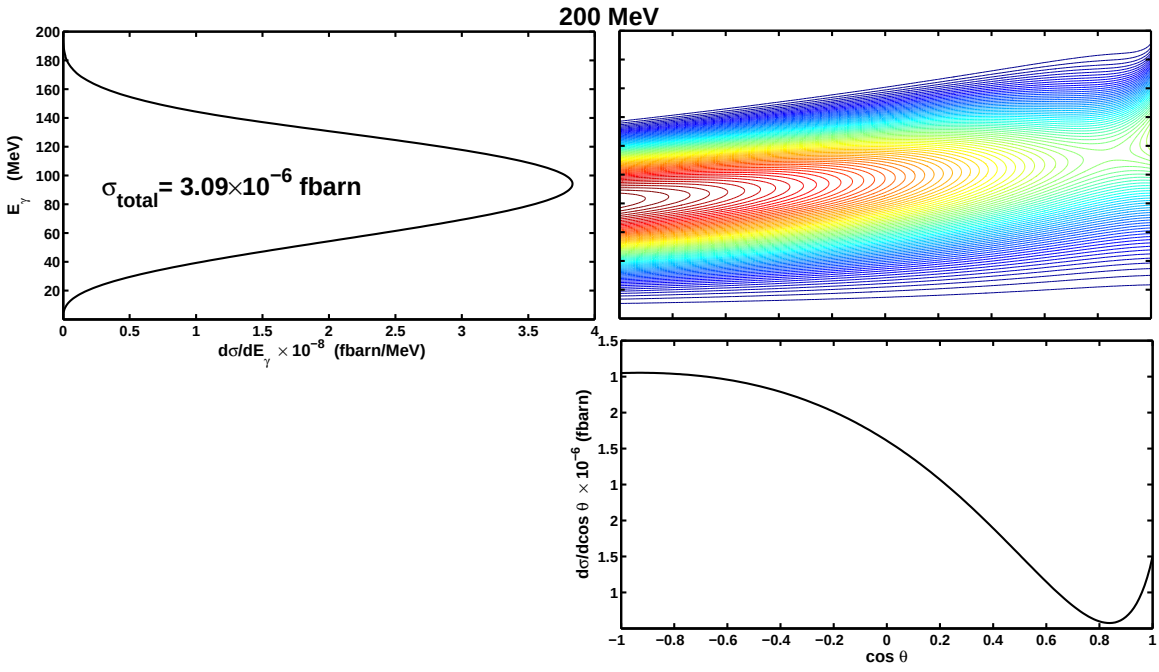

FIG. 2: Lab frame cross section with beam energy $E_{\ell_i} = 200$ MeV.

to simplify the notation. The dimensionless quantities a, b and c are all greater than unity, assuming physical parameter values. This leaves only the one-dimensional E_{ℓ_f} integral to perform.

A. Cross Section Characteristics

In the CM form, the predicted cross section is weakly peaked in the backward direction with an energy maximum near the highest allowed energies due to the overall factor of E_k. Boosting to the lab frame pushes the angular distribution forward and spreads the energy of the photon in the standard way. Numerically integrating Eq. (8), we plot the differential cross-section for beam energies of 200 MeV, 350 MeV, 500 MeV and 1000 MeV in Figs.2, 3, 4 and 5, respectively. These are boosted to the lab frame for convenience. In each case, we display the E_γ and $\cos\theta$ dependent contour plots as well as energy projection panels for the result of integrating over one of the variables. The total cross section is also noted for reference. The angular distribution moves toward the forward peak with increasing

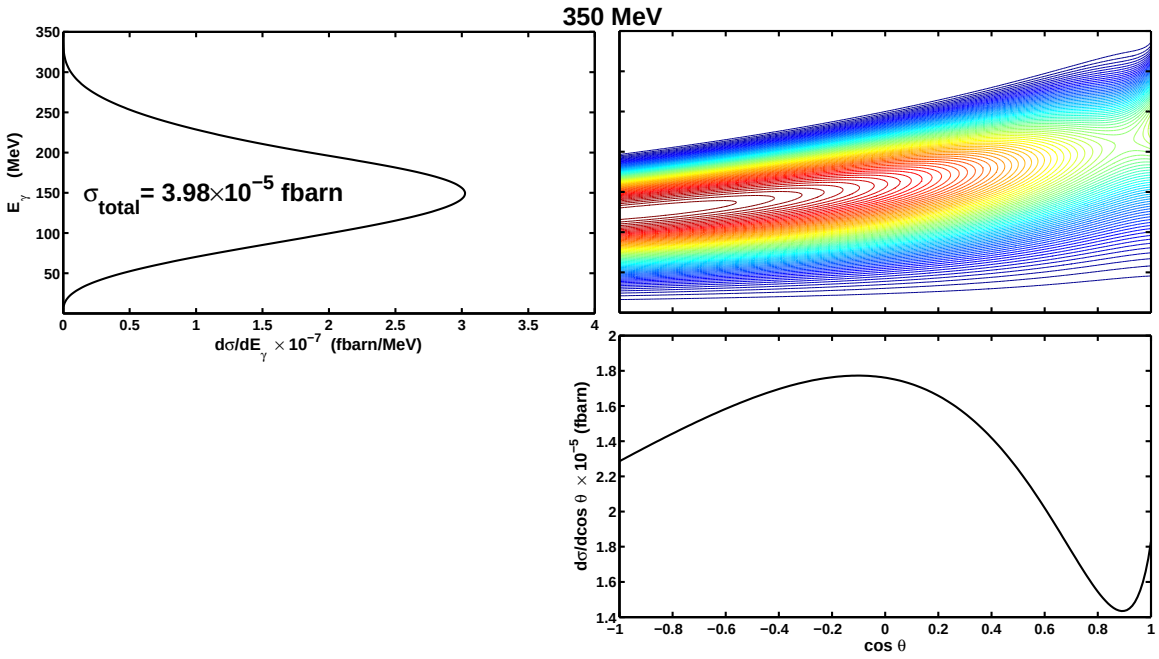

FIG. 3: Lab frame cross section with beam energy $E_{\ell_i} = 350$ MeV.

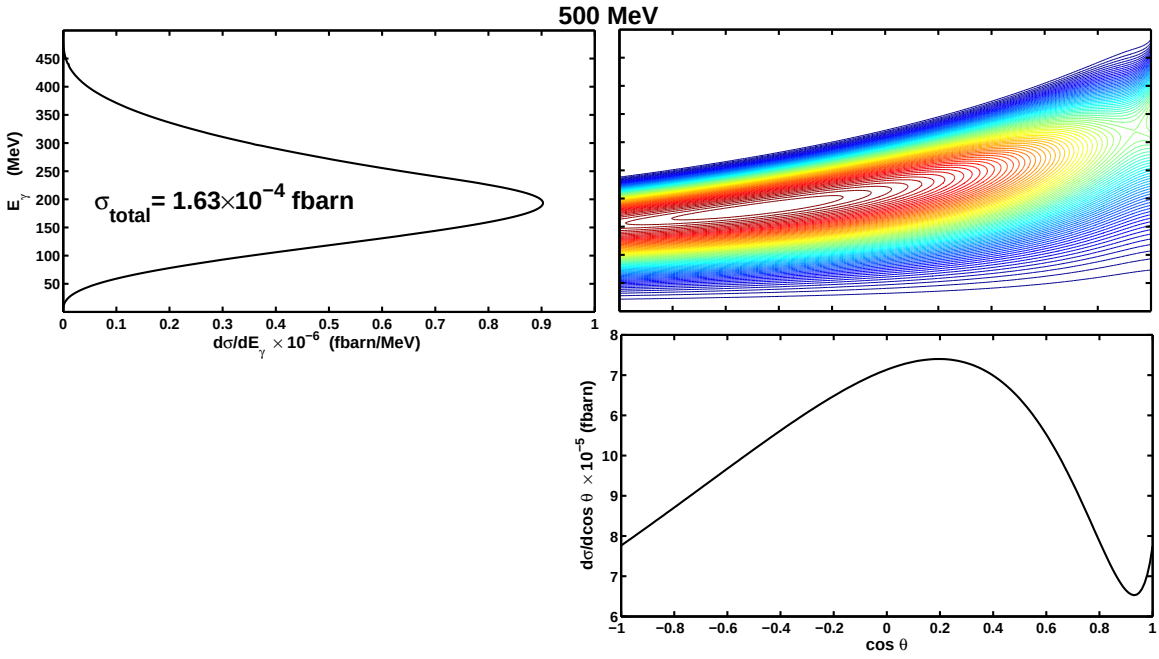

FIG. 4: Lab frame cross section with beam energy $E_{\ell_i} = 500$ MeV.

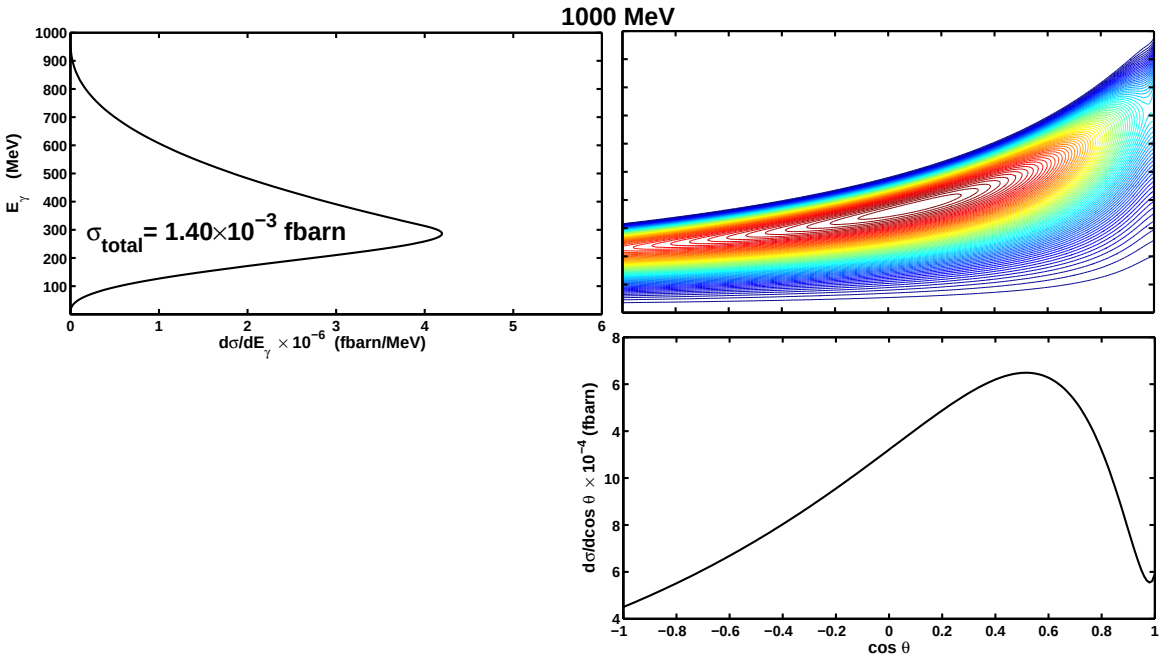

FIG. 5: Lab frame cross section with beam energy $E_{\ell_i} = 1000$ MeV.

neutrino energy due to the growing boosts from the CM to the lab frame. The distribution consistently peaks near the center of the kinematically allowed photon energy range.

Integrating over the final state photon energy and angular distribution, we plot the total cross section as a function of neutrino beam energy in Fig.6. At high energies ($E_\nu \gg M_N$) the cross section grows as $\sqrt{E_\nu}$. Near threshold, it grows as E_ν^2, as can be seen in the logarithmic low energy insert plot. In the energy region below 1000 MeV, the cross section does not exceed 10^{-3} fbarns, which is roughly three orders of magnitude less than the typical charged current cross sections at these energies [19]. Nevertheless, it is still at a level where it can affect current [2, 3] and next generation [20] experiments that probe neutrino interactions with sub-percent sensitivities. Current and proposed long baseline oscillation experiments (see, for example [21, 22, 23, 24] and references therein) will be sensitive to this class of processes with the order of magnitude enhanced cross sections shown in the high energy region of Fig.6.

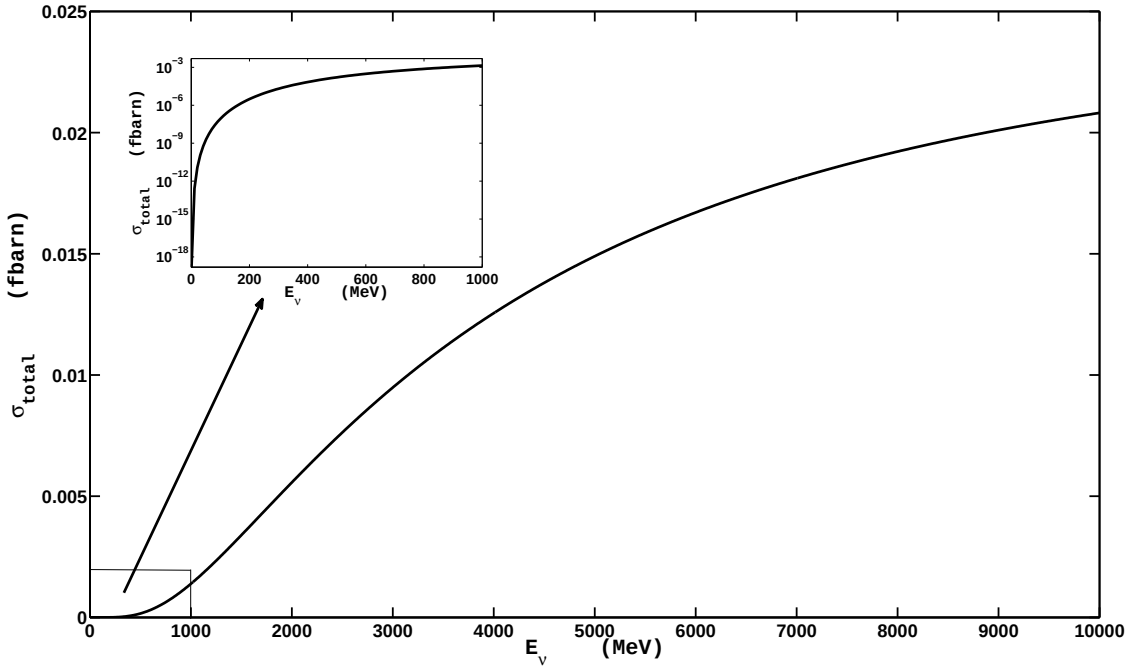

FIG. 6: Total cross section as a function of neutrino beam energy

IV. DISCUSSION

Other processes, related to that in Fig.1, such as by exchange of the ω and π^0 for other mesons (with the same quantum numbers), will contribute to similar production of photons in the final state. These will differ from our calculation here only by the meson masses and coupling constants.

We also observe that this process yields identical results for both neutrino and anti-neutrino scattering. The only difference between these resides in a sign change between the axial-vector neutrino-Z coupling. The asymmetry term vanishes when Lorentz contracted with the rest of the diagram, which is symmetric under the free indices of the vertex. (We have checked this feature by direct calculation.) This is not the case for non-radiative neutral current neutrino scattering, where there is a difference between neutrino and anti-neutrino amplitudes. Additionally, we find by means of direct computation that many variants of Fig.1 vanish due to similar symmetry reasons. In particular,

- Amplitudes from diagrams with axial vector mesons replacing the vector ω vanish.

- The amplitude of the process with the π and ω mesons interchanged is zero.
- Amplitudes from "reversed" diagrams (where the π_0 couples to the neutrino) vanish.

We have used a phenomenological on-shell coupling strength for the $\omega - \pi - \gamma$ vertex, which is a commonly used phenomenological approach. The slow off-shell variation of the computed $Z - \omega$ mixing supports such an approach, although a three-particle vertex may well behave differently. The variation one expects is for a decrease in amplitude as vertex form factors act to suppress the effective coupling [25]. This may be ultimately recovered by summing over higher mass Regge recurrences in an extension of our approach, which would eventually transition at very high energies to a purely quark picture of the couplings.

Such a view raises the question as to whether the H3 axial anomaly might not give a more reliable evaluation of the strength of these processes after all. However, the use of the anomaly is only guaranteed accurate when currents coupling to the vertices are point-like. In the case of the pion, the axial current satisfies this condition, but for the ω, being a composite object, the vector isoscalar current cannot provide the same guarantee. The vertex structure for $\omega - q - \bar{q}$ coupling produces the same kind of uncertainties in the H3 approach as we encounter here; perhaps more so as the ω momentum wavefunction in the quark basis may only be known via Lattice QCD calculations, although crude quark model calculations do produce a 3-π hadronic width consistent with experiment. [26] We believe the issue is less serious for our calculation as the $Z - \omega$ mixing is effectively used only within a region of order only a few mass squared units from the on-shell point.

Our view is that for low to modest energy scattering, such as is relevant to the experiments discussed here, our phenomenological approach is as valid as any other, although it is most reliable for momentum transfer and angular distributions, and least reliable for absolute rates. The most certain point is that these t-channel processes will be the same in neutrino and in anti-neutrino scattering, so a comparison of the two running modes for MiniBooNE will set the most stringent limits on the strength of these contributions to the total rate.

Another significant background also occurs when a neutral pion is produced instead of a photon, but one of the photons from the decay of this pion is lost to the detector. Fortunately, in this case the event rate can be normalized to the corresponding case in charged current neutrino scattering, which produces a neutral pion in conjunction with the charged lepton.

Although this may dominantly occur due to intermediate state processes, such as production of a Δ baryon or N^* followed by its decay back to a nucleon and a pion (see [27] and reference therein), concern also arises regarding other processes, including those that may be coherent over the entire nuclear target with attendant amplification of the rate [28, 29]. The approach taken above can also be applied to such calculations where again, the pion is not produced in an s-channel fashion from a nucleon or one of its N^* or Δ excited states, but from a t-channel process, corresponding to the photon production above. We will discuss that process in a separate paper.

Finally, we comment on the effect of replacing the ω by a ρ^0: For the case of ρ meson exchange (in place of the ω), the analogous plots to those displayed for ω-exchange are very similar in shape and absolute magnitude. The ratio of separate contributions depends upon both the ratios of the vector meson-pion-photon coupling constants, $g_{V-\gamma-\pi}$, estimated in the Appendix, as well as the vector meson-Z coupling constants, g_{VZ}. We estimate $\sigma^\rho/\sigma^\omega \approx (g_{\rho-\gamma-\pi}/g_{\omega-\gamma-\pi})^2 \times (g_{\rho Z}/g_{\omega Z})^2 \approx 1.6$, using parameter values taken from Ref.([30]). The suppression arises primarily from the coupling associated with the meson$-\pi-\gamma$ vertex while the enhancement is due to Z-meson mixing. See the Appendix A for more details.

The amplitudes for these processes are comparable, and significant interference is expected to be possible. From this effect the overall cross sections may be modified by a factor between 0.07 and 5.1 for total destructive and constructive interference respectively. The cross section yielded by the lower limit is well below current or expected future experimental sensitivities and therefore forms a negligible background in that case. These considerations are interesting for future work, because of the parallel process of coherent pion production: If the interference is destructive, there can be a significant difference between coherent pion production between charged and neutral current cases as this interference cannot occur in the charged current case.

In conclusion, we remark that whether the interference is constructive or destructive, our results apply equally to neutrino and to antineutrino neutral current scattering, since that only affects the overall sign of the amplitude by the neutrino coupling to the Z-boson. Thus, the process discussed here must contribute equally to neutrino and to antineutrino neutral current scattering, and with the same energy and angular dependence for the appearance of the photon.

Acknowledgments

We thank G. Garvey, W. Louis and G. Mills for discussions regarding the LSND and MiniBooNE experiments and their data. This work was carried out in part under the auspices of the National Nuclear Security Administration of the U.S. Department of Energy at Los Alamos National Laboratory under Contract No. DE-AC52-06NA25396.

After this work was completed, we learned of a complementary analysis [31] that uses effective field theory techniques, rather than the phenomenological approach taken here. The results are similar in character.

---

[1] A. Aguilar et al. (LSND), Phys. Rev. **D64**, 112007 (2001), hep-ex/0104049.

[2] A. A. Aguilar-Arevalo et al. (The MiniBooNE), Phys. Rev. Lett. **98**, 231801 (2007), 0704.1500.

[3] A. A. Aguilar-Arevalo et al. (MiniBooNE) (2009), 0903.2465.

[4] W. J. Marciano and A. Sirlin, Phys. Rev. Lett. **71**, 3629 (1993).

[5] J. T. Goldman and W. J. Wilson, Phys. Rev. **D15**, 709 (1977).

[6] E. A. Choban and V. M. Shekhter, Yad. Fiz. **26**, 1064 (1977).

[7] S. S. Gershtein, Y. Y. Komachenko, and M. Y. Khlopov, Sov. J. Nucl. Phys. **33**, 860 (1981).

[8] P. Alibran et al. (Gargamelle), Phys. Lett. **B74**, 422 (1978).

[9] G. Garvey, private communication (2009).

[10] D. Rein and L. M. Sehgal, Phys. Lett. **B104**, 394 (1981).

[11] S. Agostinelli et al. (GEANT4), Nucl. Instrum. Meth. **A506**, 250 (2003).

[12] D. Casper, Nucl. Phys. Proc. Suppl. **112**, 161 (2002), hep-ph/0208030.

[13] S. L. Adler, Ann. Phys. **50**, 189 (1968).

[14] J. A. Harvey, C. T. Hill, and R. J. Hill, Phys. Rev. Lett. **99**, 261601 (2007), 0708.1281.

[15] D. Schildknecht, Acta Phys. Polon. **B37**, 595 (2006), hep-ph/0511090.

[16] K. F. Liu, S. J. Dong, T. Draper, and W. Wilcox, Phys. Rev. Lett. **74**, 2172 (1995), hep-lat/9406007.

[17] J. T. Goldman, J. A. Henderson, and A. W. Thomas, Few Body Syst. **12**, 123 (1992).

[18] J. T. Goldman, J. A. Henderson, and A. W. Thomas, Mod. Phys. Lett. **A7**, 3037 (1992).

[19] P. Lipari, M. Lusignoli, and F. Sartogo, Phys. Rev. Lett. **74**, 4384 (1995), hep-ph/9411341.

[20] H. Chen et al. (MicroBooNE) (2007).

[21] P. Adamson et al. (MINOS), Phys. Rev. Lett. **101**, 131802 (2008), 0806.2237.

[22] D. S. Ayres et al. (NOvA) (2004), hep-ex/0503053.

[23] M. Aoki et al., Phys. Rev. **D67**, 093004 (2003), hep-ph/0112338.

[24] D. Beavis et al. (2002), hep-ex/0205040.

[25] J. P. Lansberg, AIP Conf. Proc. **892**, 324 (2007), hep-ph/0610393.

[26] A. Dar and V. F. Weisskopf, Phys. Lett. **26B**, 670 (1968).

[27] E. A. Paschos, L. Pasquali, and J. Y. Yu, Nucl. Phys. **B588**, 263 (2000), hep-ph/0005255.

[28] E. Isiksal, D. Rein, and J. G. Morfín, Phys. Rev. Lett. **52**, 1096 (1984).

[29] D. Rein and L. M. Sehgal, Nucl. Phys. **B223**, 29 (1983).

[30] W. M. Yao et al. (Particle Data Group), J. Phys. **G33**, 1 (2006).

[31] R. J. Hill (2009), 0905.0291.

APPENDIX A: SUBSIDIARY ISSUES

For completeness, we show the explicit calculations of the decay rate for the ω and the $Z-\omega$ mixing amplitude.

1. $\Gamma(\omega \to \pi + \gamma)$

We calculate the ω decay width $\Gamma(\omega \to \pi + \gamma)$ from the phenomenological vertex $\mathcal{L}_{\mathcal{I}} = e g_{\omega\gamma\pi} \epsilon_{\mu\nu\xi\sigma} \omega^{\mu} \partial^{\nu} \pi^{0} F^{\xi\sigma}$. This same form arises in the triangle anomaly considered in H3. Neglecting the π^0 mass, the squared amplitude of this process is

$$\mathcal{A}^2 = -\frac{2e^2 g_{\omega\gamma\pi}^2}{3} k \cdot q = \frac{e^2 g_{\omega\gamma\pi}^2 M_{\omega}^4}{6}, \tag{A1}$$

where k and q are the photon and pion momenta, respectively. Evaluating the decay width yields

$$\Gamma(\omega \to \pi + \gamma) = \frac{\alpha g_{\omega\gamma\pi}^2 M_{\omega}^3}{24}. \tag{A2}$$

Fitting this to the observed decay width [30], we extract the coupling constant $g_{\omega\gamma\pi} = 1.8/M_{\omega}$, which we use in the numerical examples throughout our analysis. Evaluat-

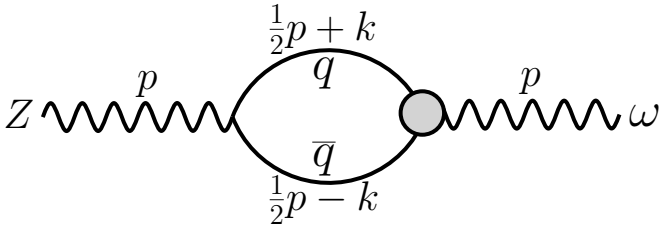

FIG. 7: Self energy diagram leading to $Z-\omega$ mixing.

ing the tree diagram without the Lorentz structure of the anomaly yields $g_{\omega\gamma\pi} \sim 1.2/M_\omega$, i.e., a factor of 2/3 smaller than is obtained from Eq. (A2). These are written in the form of a dimensionless coupling relative to the ω mass to help illustrate the scale associated with the effective vertex and strong coupling strength. A similar exercise may be performed with the ρ^0 decay, in which case one extracts $g_{\rho\gamma\pi} = 0.55/M_\rho$.

2. p^2 dependence of the $Z-\omega$ mixing amplitude

The p^2 dependence of the $Z-\omega$ mixing coefficient $g_{\omega Z}(p^2)$ may be found from the self-energy diagram shown in Fig.7. Following references ([17, 18]), we parameterize the $\omega - q\bar{q}$ vertex by the form factor $g_{\omega q\bar{q}} M^2/(M^2-p^2)$, where the $g_{\omega q\bar{q}} \approx 3.1$ coupling is extracted from $\omega \to \pi^0\,\pi^+\,\pi^-$ decay measurements [30], under the usual quark model assumption that inclusive processes may be well-approximated with the use of quark-hadron duality. The scale, M, defines the finite substructure of the ω meson. Evaluating this diagram, we find the self-energy

$$\begin{aligned}\Pi_{\mu\nu} &= \frac{-8igg_{\omega q\bar{q}} M^2 \sin^2\theta_W}{3(2\pi)^d \cos\theta_W} \int_0^1 dxdydz\delta(x+y+z-1) \\ &\times \int d^d\ell \frac{\left(1-\frac{2}{d}\right)\ell^2\eta_{\mu\nu} + z(z-1)\left(p^2\eta_{\mu\nu} - 2p_\mu p_\nu\right) + m_q^2\eta_{\mu\nu}}{\left(\ell^2 - p^2 z(z-1) - m_q^2(y+z) - M^2 x\right)^3},\end{aligned} \tag{A3}$$

where the d-dimensional integral is written to aid in the renormalization of the divergent ℓ^2 term via dimensional regularization and m_q is the average light quark mass. Considering only the terms that contribute to the p^2 dependence of $\omega - Z$ mixing and dropping logarithmic contributions, we find

$$g_{\omega Z}(p^2) = \frac{-gg_{\omega q\bar{q}} M^2 \sin^2\theta_W}{12\pi^2\cos\theta_W} \int_0^1 dz \int_0^{1-z} dx \frac{p^2 z(z-1) + m_q^2}{p^2 z(z-1) + m_q^2 + x(M^2 - m_q^2)}. \tag{A4}$$

Taking the reasonable limit $m_q^2 \ll M^2,\ p^2$, we evaluate the above integral to yield

$$g_{\omega Z}(p^2) \approx \frac{g g_{\omega q\bar{q}} M^2 \sin^2\theta_W}{72\pi^2 \cos\theta_W} \frac{1}{\eta^2} \left\{ 2\eta(1-\eta) + (2-3\eta)\ln(1-\eta) + \eta^3 \ln\left(\frac{1-\eta}{-\eta}\right) \right. \tag{A5}$$
$$\left. + \epsilon \left(\eta(4-\eta) + (4-3\eta)\ln(1-\eta) - \eta^2(6+\eta)\ln\left(\frac{1-\eta}{-\eta}\right) \right) + \mathcal{O}(\epsilon^2) \right\},$$

with the dimensionless quantities, $\eta = p^2/M^2$ and $\epsilon = m_q^2/M^2$. For the $p^2 < 0$ range relevant to this analysis, $g_{\omega Z}(p^2)$ is real. The ϵ correction term is well-behaved and negligible for realistic parameter values where $\epsilon \sim 10^{-5}$. The leading order term of Eq. (A5) breaks down for $-p^2 < 1$ MeV^2 or $-\eta < 1.6 \times 10^{-6}$. The limiting behavior of $g_{\omega Z}(p^2)$ is easy to extract and is useful in estimating the physical parameter range

$$g_{\omega Z}(p^2) = \frac{g g_{\omega q\bar{q}} M^2 \sin^2\theta_W}{24\pi^2 \cos\theta_W} \begin{cases} -\left(1 + \frac{\ln(-\eta)}{\eta}\right) + \mathcal{O}\left(\frac{1}{\eta}\right) & (-\eta \gg 1) \\ \frac{1}{3}(1 - \eta\ln(-\eta)) + \mathcal{O}(\eta) & (-\eta \ll 1) \end{cases}. \tag{A6}$$

For the neutrino beam energies studied here between $200 - 1000$ MeV, we find that the average coupling $\bar{g}_{\omega Z} = 600$ MeV^2, under the assumptions that $m_q \sim 3$ MeV [30] and $M \sim M_\omega$.

3. Relative strengths of $Z-\rho$ and $Z-\omega$ mixing

On the basis of $SU(3)$ flavor symmetry, one expects a similar result for the ρ^0, except for the effect of isospin. In Fig.(7), the ω couples equally to the u and d quarks that contribute to the loop, which weights the $Zq\bar{q}$ couplings, viz.

$$g_{Zu\bar{u}} = \frac{g}{4\cos\theta_W}\left(\frac{8}{3}\sin^2\theta_W - 1\right) \tag{A7}$$

$$g_{Zd\bar{d}} = \frac{g}{4\cos\theta_W}\left(1 - \frac{4}{3}\sin^2\theta_W\right) \tag{A8}$$

equally, whereas the ρ^0 does so with opposite signs due to isospin. (The γ_5 parts of the couplings are omitted as irrelevant; they cannot contribute to the mixing since there is only one momentum available to combine with the 4-dimensional Levi-Civita tensor that comes from the fermion trace.) As might be expected from the fact that the Z-boson is dominantly isospin 1 like the ρ, the $Z-\rho$ mixing is enhanced relative to the $Z-\omega$ mixing.

Combining these considerations with the slight phenomenological deviation from $SU(3)$ flavor symmetry yields

$$\begin{aligned} \frac{g_{\rho Z}}{g_{\omega Z}} &= \frac{g_{Zd\bar{d}} - g_{Zu\bar{u}}}{g_{Zd\bar{d}} + g_{Zu\bar{u}}} \times \frac{g_{\rho q\bar{q}}}{g_{\omega q\bar{q}}} \\ &\sim 3\frac{1-2\sin^2\theta_W}{2\sin^2\theta_W} \times \sqrt{\frac{\Gamma(\rho\to\pi\pi)}{\Gamma(\omega\to\pi\pi\pi)}\frac{\phi(\omega\to\pi\pi\pi)}{\phi(\rho\to\pi\pi)}} \\ &= 4.1, \end{aligned} \tag{A9}$$

where ϕ denotes the phase space integral for the decay, which suppresses the ratio by approximately $\sqrt{4\pi}$. We take the numerical value of $\sin^2\theta_W \sim 0.2396$ from the Particle Data Group extrapolation to small four-momentum transfer [30]. The effect of this enhancement is included in our final discussion.